

Article

# Permeability of High Clay Content Dredger Fill Treated by Step Vacuum Preloading: Pore Distribution Analysis

Wenchong Shan, Xiaoqing Yuan \*, Hui-e Chen, Xiaolin Li and Jinfeng Li

College of Construction Engineering, Jilin University, Changchun 130026, China; shanwc19@mails.jlu.edu.cn (W.S.)

\* Correspondence: yuanxiaoqing@jlu.edu.cn; Tel.: +86-137-5656-7311

**Abstract:** In this study, the step vacuum preloading method was used to reinforce high clay content dredger fill in the laboratory. The pore structures and permeability characteristics of dredger fill under different vacuum pressures were tested. The correlation between the pore structure parameters and permeability coefficient was analyzed using the grey T's correlation analysis method. The research results indicate that the pore ratio, large pore (the diameter with a range of 4–40  $\mu\text{m}$ ) content, and permeability coefficient of dredger fill decreased with the increase in vacuum pressures, but the decrease rates of the pore ratio were different at various sampling locations. The contents of micropores (the diameter with a range of  $<0.04 \mu\text{m}$ ) and small pores (the diameter with a range of 0.04–0.4  $\mu\text{m}$ ) increased with the increase in vacuum pressure. The results of the correlation analysis showed that a large pore content had a strong correlation with the permeability coefficient and could be used to describe the permeability characteristics of soil. The research results can provide reference for the improvement of the reinforcement method and for the evaluation of the reinforcement effect of dredger fill in engineering practice.

**Keywords:** step vacuum preloading; high-clay content dredger fill; pore distribution; permeability; correlation analysis



**Citation:** Shan, W.; Yuan, X.; Chen, H.-e.; Li, X.; Li, J. Permeability of High Clay Content Dredger Fill Treated by Step Vacuum Preloading: Pore Distribution Analysis. *J. Mar. Sci. Eng.* **2023**, *11*, 1714. <https://doi.org/10.3390/jmse11091714>

Academic Editor: José António Correia

Received: 19 July 2023

Revised: 20 August 2023

Accepted: 25 August 2023

Published: 30 August 2023



**Copyright:** © 2023 by the authors. Licensee MDPI, Basel, Switzerland. This article is an open access article distributed under the terms and conditions of the Creative Commons Attribution (CC BY) license (<https://creativecommons.org/licenses/by/4.0/>).

## 1. Introduction

When the traditional vacuum preloading method is used to consolidate high clay content dredger fill, the drainage capacity of the prefabricated vertical drain (PVD) will be weakened [1–3] due to the blockage caused by fine particles. Based on the vacuum preloading method, the step vacuum preloading (SVP) is applied to solve the problem [4–8]. Before the application of vacuum pressure, the dredger fill to be treated is characterized by a higher moisture content, higher porosity, and lower strength. After being reinforced, the soil will have a certain bearing capacity and its permeability will be changed greatly [9]. The permeability coefficient is an important parameter to evaluate the consolidation effects and the property of soil [10,11].

With the rapid development of reclamation engineering, the permeability features of soil treated by the vacuum preloading method have been studied extensively in recent years [12–18]. The influence of permeability on settlement has been discussed for the accurate prediction of settlement and proper evaluation of the reinforcement effect of the soil. Based on field data, Zhuang et al. [10] established a numerical model to analyze the relationship between the settlement and the permeability coefficient of a stabilized soft soil site. Wu et al. [9] discussed the change in permeability coefficient with depths and locations from the PVD after the dredger fill was treated by the laboratory vacuum preloading method. Li et al. [19] adopted a five-level (10, 20, 40, 60, and 80 kPa) vacuum preloading plan on a dredger fill in the laboratory. During the test, the permeability coefficients, pore ratio, settlement, and pore water pressure of the soil were measured. The results proved that the SVP was effective at reinforcing dredger fill with high clay content. The permeability

of soil is controlled by its pore characteristics [20–23], and the flow of fluid in soil is determined by the geometric spatial characteristics of the pores. Porosity is the primary factor affecting the permeability of soil, and pore size distribution plays an important role in fluid flow in soil [24–27]. During the process of SVP, the characteristics of pores change significantly, causing the permeability of the dredger fill to change accordingly. So, it is necessary to analyze the permeability of soil from the aspect of pore characteristics. At present, many scholars have investigated the pore characteristics of soil treated by vacuum preloading, and have discussed the changes of porosity [28,29], pore size distribution [30], and pore directionality [31] during reinforcement. However, the study on the dynamic change of permeability coefficient during vacuum preloading process from the aspect of pore features is limited, the correlations between the pore parameters and permeability during the SVP process have seldom been studied. Therefore, it is necessary to study the evolution mechanism of permeability characteristics for dredger fill treated by the SVP method, so as to provide a reference for the improvement of the SVP method and for the evaluation of the consolidation efficiency of dredger fill.

In this study, SVP was used to treat high clay content dredger fill in the laboratory. During the consolidation process, the pore features changed all the time. Correspondingly, the permeability characteristics of the dredger fill changed. To clarify the variation of pore parameters and permeability with time and space during the SVP process, a mercury intrusion porosimetry test (MIP) and permeability test were conducted on samples obtained at different times and from the different locations of the test bucket. Then, the relationship between pore parameters and permeability coefficient of the soil was analyzed.

## 2. Materials and Methods

### 2.1. Sample Properties

The studied soil was obtained from Nangang Industrial Zone, Binhai New Area in Tianjin (Figure 1). The site was filled in 2016 and not subjected to any reinforcement process. The dredger fill had a thickness of 8–9 m in the sampling location, and its properties were relatively uniform. During sampling, the surface hard layer was removed first, and the soils with original moisture content of 30–80% were dug and put into a bag. The sampling depth was 1 m.

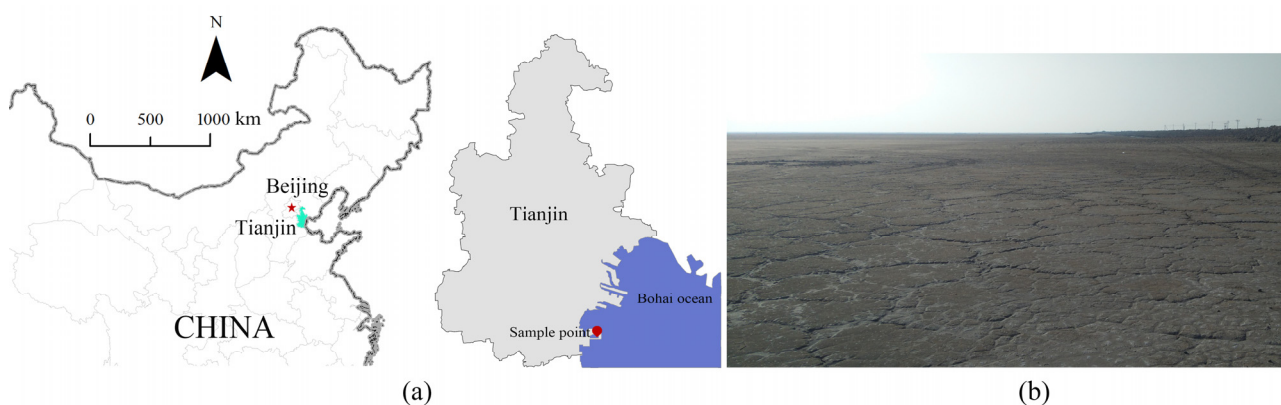


**Figure 1.** Sampling location: (a) Map of Tianjin, China; (b) realistic view of sampling location.

The soluble salt content of the soil is listed in Table 1. The total soluble salt content was 1.756%, and the main ions were  $\text{Na}^+$  and  $\text{Cl}^-$ . The basic properties of the soil are showed in Table 2. The content of clay particles was more than 50%, so the soil belonged to high-clay content dredger fill. According to the ASTM D2487-17, the soil was classified as lean clay. The mineral compositions of the soil were measured by X-ray diffraction analysis, and the results are shown in Figure 2. Quartz had the highest content of 36.1%, followed by the illite-smectite mixed layer (I/S).

**Table 1.** Soluble salt content of the soil.

| Component      | Total                  | K <sup>+</sup>   | Na <sup>+</sup> | Cl <sup>-</sup>          | Ca <sup>2+</sup>       | Mg <sup>2+</sup> | SO <sub>4</sub> <sup>2-</sup> | CO <sub>3</sub> <sup>2-</sup> | HCO <sub>3</sub> <sup>-</sup> |
|----------------|------------------------|------------------|-----------------|--------------------------|------------------------|------------------|-------------------------------|-------------------------------|-------------------------------|
| Percentage (%) | 1.756                  | 0.029            | 0.525           | 0.951                    | 0.016                  | 0.022            | 0.156                         | 0.000                         | 0.025                         |
| Method         | Water bath evaporation | Flame photometer |                 | Silver nitrate titration | EDTA complex titration |                  |                               | Neutralisation titration      |                               |

**Table 2.** Basic properties of the soil.

| Granulometric Composition     |             |         | Physical Properties           |               |               |           |
|-------------------------------|-------------|---------|-------------------------------|---------------|---------------|-----------|
| Size Fraction (mm) Percentage |             | Density | Liquid Limit                  | Plastic Limit | Plastic Index |           |
| >0.075                        | 0.005–0.075 | <0.005  | $\rho_s$ (kg/m <sup>3</sup> ) | $w_L$ (%)     | $w_P$ (%)     | $I_P$ (%) |
| 0.09%                         | 47.91%      | 52.06%  | 2740                          | 44.62         | 26.38         | 18.24     |

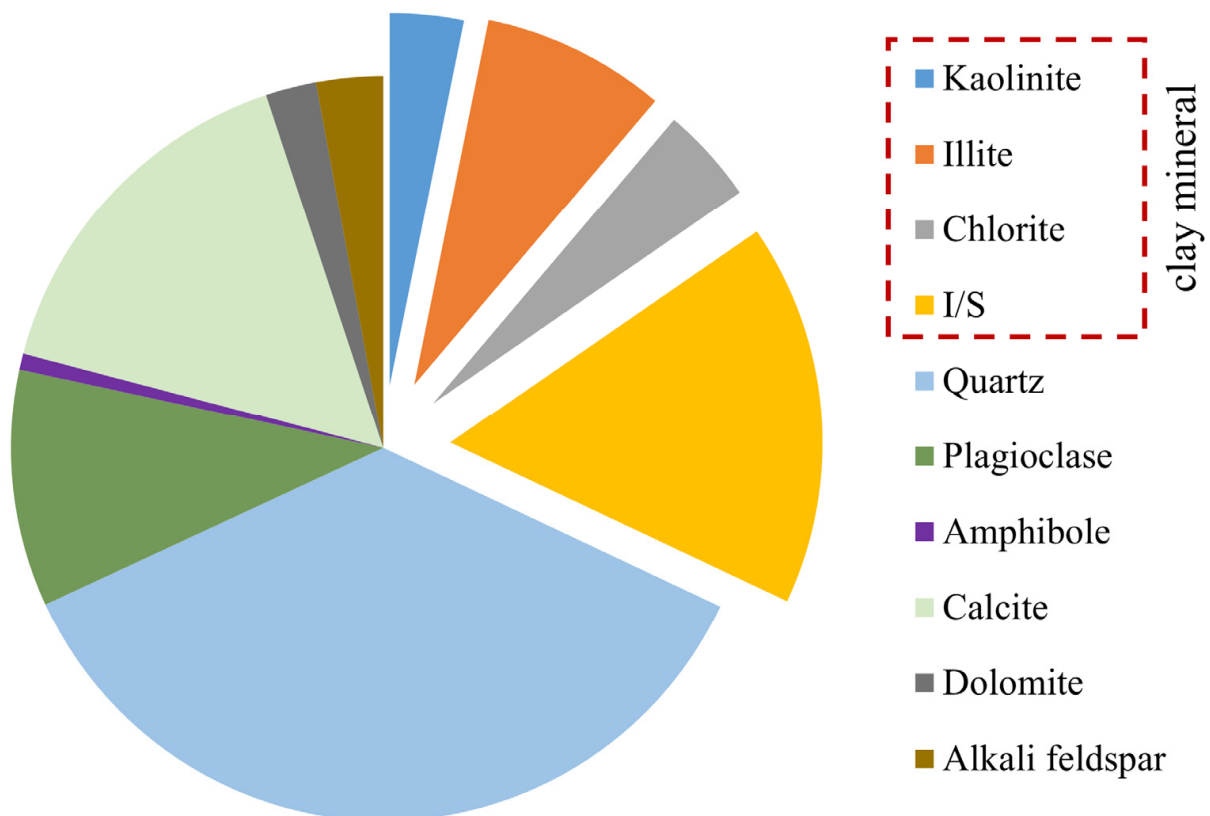


**Figure 2.** Mineral composition of the dredger fill.

### 2.2. SVP Model Test

The equipment used for the SVP test was a self-designed bucket. Figure 3 shows its schematic diagram. Two pore water pressure gauges were arranged at different positions of the bucket bottom. In the inner wall of the bucket, the settlement gauge was installed to monitor the settlement of the soil surface. A vacuum gauge was installed at the center of PVD to determine the vacuum pressure of the SVP test. Water collection devices were used to measure the displacement. The testing soil was sealed by a sealing film, and the vacuum pump, sealing film, and soil–water separator worked together to control the levels of vacuum pressure (through Valve 3 of the soil–water separator). The test has been described in detail by Shan et al. [8] and Li et al. [19].

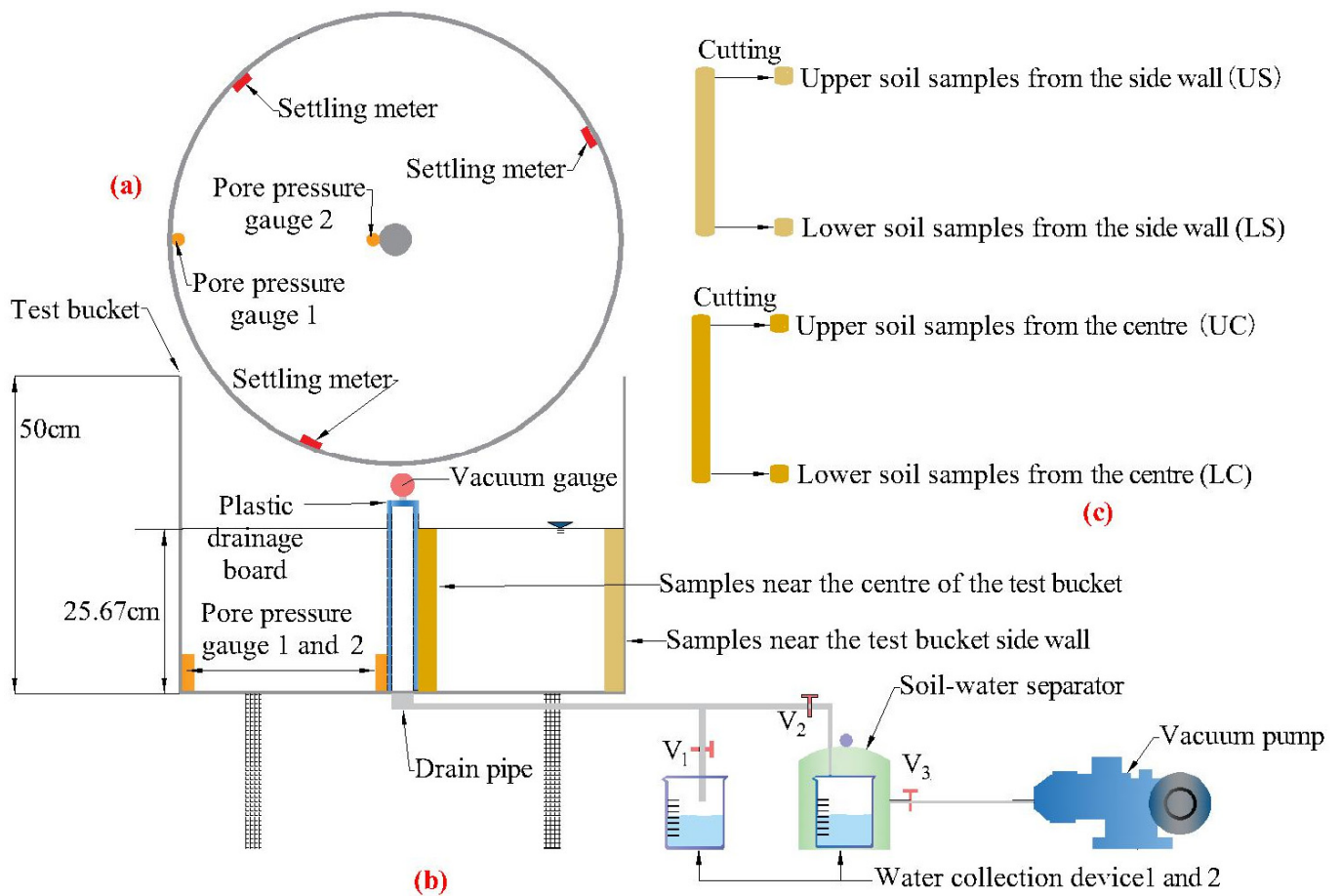


**Figure 3.** Test equipment and sampling positions: (a) plan view of the SVP test equipment; (b) front view of the SVP test equipment and sampling positions; (c) sampling positions.

The original soil underwent a natural sedimentation process in which some of the water was discharged. So, the moisture content of the soil was uneven. According to the study of Yuan et al. [4,28], the moisture content of the sample used in the SVP test was controlled as 120%. The SVP test lasted for 117 days. The corresponding time nodes of each experimental stage are shown in Figure 4a. There were two stages in the SVP test, namely, self-weight consolidation (SWC) stage and step vacuum pressure loading stage. The SWC stage included soil–water separation and self-weight sedimentation processes [32]. During the step vacuum pressure loading stage, five-level vacuum pressures (10, 20, 40, 60, and 80 kPa) were applied to consolidate the dredger fill.

**SWC stage:** As shown in Figure 4b, the soil sample was in a mud state at the beginning of the test. The initial height of the mud was 25.67 cm. At this stage, no water was drained, and the total weight of the mud remained unchanged. As time went on, the water and soil began to separate (Figure 4c), and this stage finished when the positions of water and soil surface and the readings of pore water pressure gauges were unchanged. After opening Valve 1, water was discharged through the PVD under gravity, and the stage of self-weight sedimentation started (Figure 4d). The ending criterion of this stage was the same as the soil–water separation stage. As the SWC stage finished, soil samples for the MIP test were taken from the UC, US, LC, and LS, as shown in Figure 3c.

**Step vacuum pressure loading stage:** five-level vacuum pressures (10 kPa to 20 kPa to 40 kPa to 60 kPa to 80 kPa) were applied to treat the dredger fill. Under a certain level of vacuum pressure, when the settlement of soil was stable and the pore water pressure changed from a stable state to a gradual increase, the vacuum pressure was then increased to the next level.

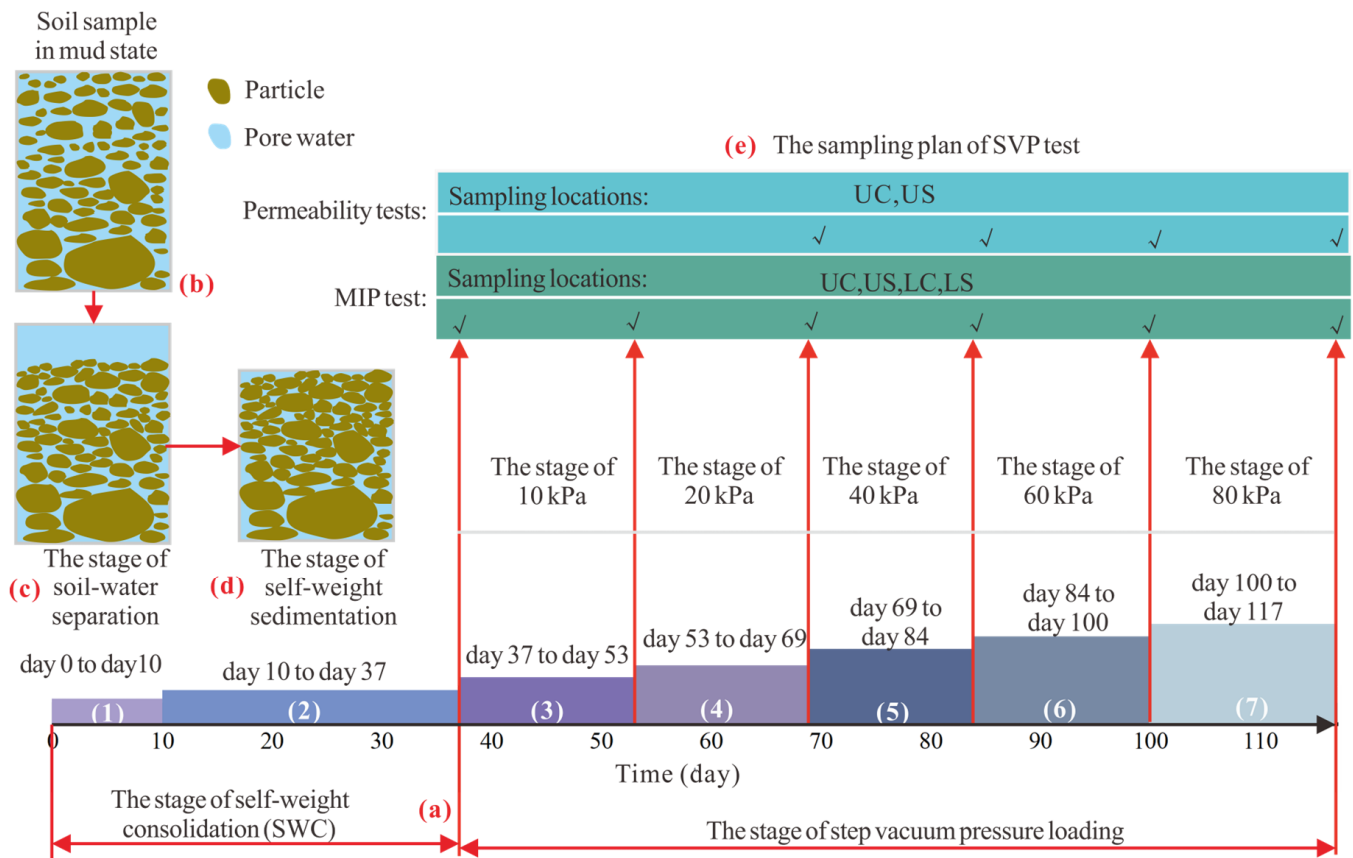


**Figure 4.** The experimental process and plan of SVP test: (a) the experimental process of SVP test; (b) SWC stage—the initial state of testing mud; (c) SWC stage—the stage of soil-water separation; (d) SWC stage—the stage of self-weight sedimentation; (e) vacuum pressure loading stage—the sampling plan for MIP test and permeability test.

The sampling plan for the MIP test and permeability test are shown in Figures 3c and 4e. It was difficult to collect samples for permeability test when the soil had a high moisture content. So, sampling was carried out from UC and US after the application of vacuum pressures of 20, 40, 60, and 80 kPa. The test stages and sampling plan are illustrated in Figure 4.

### 2.3. MIP Test

When the moisture content of the soil was high, it was difficult to prepare undisturbed specimens for the MIP test using traditional sampling methods. A self-designed and tried-and-tested sampler was used to prepare the specimens for the MIP test. Yuan et al. [28] demonstrated that the sampler could obtain the undisturbed soil samples with a high moisture content. We cut the samples into cylinders about 10 mm long with steel knives soaked in liquid nitrogen, and then frozen them in liquid nitrogen for 2 h. After being completely dried by a vacuum dryer, the samples were trimmed into cubes with a length of 10 mm, as shown in Figure 5b.

The MIP tests were carried out with an AutoPore IV 9500 Porosimeter (manufactured by Micromeritics Instrument Corporation, Norcross, GA, USA) (Figure 5a). Under different pressures, mercury entered the pores with different diameters. The volumes of injection mercury under each increment of pressure were recorded, and the pore diameters were calculated through Equation (1).

$$P = \frac{4\gamma \cos \theta}{d} \tag{1}$$

where  $d$  is the diameter of the pore,  $\gamma$  is the surface tension of mercury,  $\theta$  is the contact angle between the particle and mercury, and  $P$  is the pressure.



**Figure 5.** Instrument and sample for MIP and SEM test: (a) AutoPore IV 9500 Porosimeter; (b) the sample for the MIP test.

#### 2.4. Method of Correlation Analysis

The correlation analysis between the pore characteristics and permeability coefficient was carried out using Grey T's correlation analysis method. The basic idea of this method was to calculate the correlation level ( $r$ ) according to the proximity of the relative change trend of the time series curves of factors, where the relative change trend refers to the ratio of the slope of curves of reference series and comparison series in the adjacent time period [33]. The positive or negative values of  $r$  did not indicate the magnitude, but only indicate whether the change trend of the comparison sequence and the reference sequence was consistent over time.

The method is described as follows:

$$\zeta(X_i(k)) = \begin{cases} \text{sgn}(\Delta y_1(k) \cdot \Delta y_2(k)) \cdot \frac{\min(|\Delta y_1(k)|, |\Delta y_2(k)|)}{\max(|\Delta y_1(k)|, |\Delta y_2(k)|)} \\ 0(\Delta y_1(k) \cdot \Delta y_2(k) = 0) \end{cases} \quad (2)$$

$$r(X_1, X_2) = \frac{1}{n-1} \sum_{k=2}^n \zeta(X_i(k)) \quad k = 2, 3, \dots, n, \quad i = 1, 2 \quad (3)$$

In Equation (2),

$$\Delta y_i = \{\Delta y_i(k) = y_i(k) - y_i(k-1), \quad k = 2, 3, \dots, n\}, \quad i = 1, 2 \quad (4)$$

$$y_i = \{(X_i(k) - X_i(k-1))/D_i, \quad k = 1, 2, \dots, n\}, \quad i = 1, 2 \quad (5)$$

$$D_i = \sum_{k=2}^n |X_i(k) - X_i(k-1)| / (n-1), \quad i = 1, 2; \quad k = 2, 3, 4, \dots, n \quad (6)$$

where  $X$  is the study sequence.  $y$  is the sequence after standardization.  $\Delta y$  is the increment sequence.  $\zeta$  is the correlation coefficient between sequences.  $r$  is the correlation level between the reference sequence and comparison sequence.

### 3. Results

#### 3.1. Permeability Characteristics of Dredger Fill under Step Vacuum Pressures

The TST-55 permeameter (Nanjing Soil Instrument Factory Co., Ltd., Nanjing City, Jiangsu Province, China) was used for the permeability test. The permeability coefficient is calculated using Equation (7).

$$k = \frac{QL}{Aht} \quad (7)$$

where  $k$  is permeability coefficient,  $Q$  is the amount of seepage within time  $t$ ,  $L$  is the length of seepage path,  $A$  is the cross-section area of the tested sample, and  $h$  is the height of the sample.

Figure 6 illustrates the permeability coefficients of the samples obtained from the soil under different SVP stages. It shows that the permeability coefficients present a decreasing tendency with the increase in vacuum pressure. At the end of 20 kPa vacuum pressure, the permeability coefficients of the UC and US samples were  $5.46 \times 10^{-8}$  and  $8.12 \times 10^{-8}$  m/s, respectively. When the vacuum pressure was 40 kPa, the permeability coefficients of UC and US both decreased significantly. With the vacuum pressure increased to 60 and 80 kPa, the permeability coefficients decreased slowly. During the SVP test, the permeability coefficient of the central soil sample was lower than that of the soil sample at the edge of test bucket. At the end of 80 kPa vacuum pressure, the permeability coefficients of the UC and US samples were  $4.33 \times 10^{-11}$  m/s and  $1.88 \times 10^{-10}$  m/s, respectively.

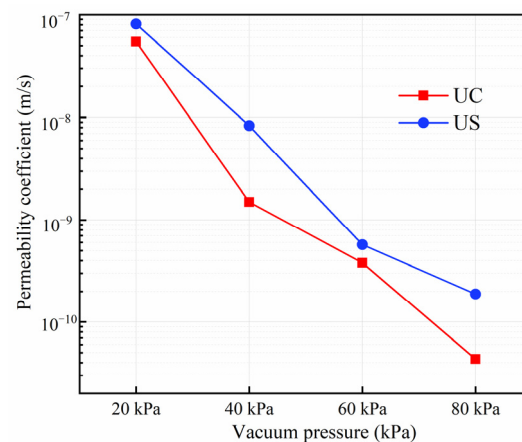


Figure 6. The permeability coefficients of the soil samples.

Under vacuum pressure, the soil near the PVD was consolidated first. Because of the long seepage path and hysteresis of vacuum pressure transmission, the soil near the side wall was consolidated slowly, resulting in a larger permeability coefficient for the US sample. During the SVP course, there was little difference in permeability coefficient between UC and US, indicating that the drainage capacity of the soil was almost the same.

#### 3.2. Pore Ratio and Pore Size Distribution Analysis

Pore characteristics have an influence on the permeability of soil [25,26,34,35]. In the study, the pore features of the treated soil were analyzed from the aspects of pore ratio and pore size distribution.

##### 3.2.1. Pore Ratio

According to the results of the MIP tests, the porosity ( $n$ ) of the testing sample could be directly obtained, and its value was the percentage of the pore volume to the total volume

of the testing sample. In engineering practice, pore ratio ( $e$ ), the volume ratio of all the pores in the soil to the skeleton particles, is often used to describe the pore characteristics of soil. Figure 7 illustrates the pore ratio of the different samples. It decreased with time. At a certain time, the pore ratio of UC was the smallest, and the pore ratio of LS was the largest.

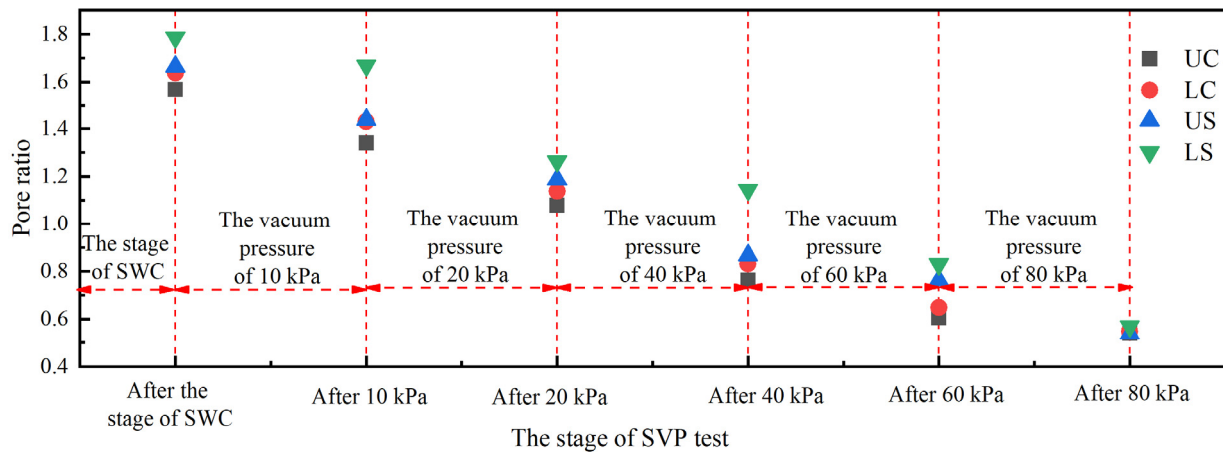


**Figure 7.** The pore ratio of the soil samples.

As the vacuum pressure increased from 0 to 40 kPa, the pore ratio of UC, LC, and US decreases rapidly. With the continuous increase in vacuum pressure, the pore ratio of the three sampling locations began to decrease at a lower rate. The pore ratio of LS decreased generally, and its decrease rate under the vacuum pressure of 60 and 80 kPa was the fastest, compared with the data of the other three sampling locations. When the stage of 80 kPa vacuum pressure ended, the pore ratio of the four sampling locations was almost the same, which was about 0.55, indicating that the SVP had a good consolidation effect on the high clay content dredger fill.

In the SVP test, the PVD was not only the seepage channel for water, but also the transmission channel for vacuum pressure. During the stage of SWC, the separated water on the upper soil discharged quickly through the PVD, leading to a small pore ratio of UC, which had been found and studied by Walker and Indraratna [36]. When the separated water was discharged completely, the vacuum pressure was loaded on the upper soil through the PVD. With the application of step vacuum pressure, the soil near the PVD consolidated first, causing the pore ratio of LC and UC to be small. Additionally, the upper soil was in contact with the sealing film, and the soil of US underwent vacuum pressure earlier than the soil of LS, leading to a smaller pore ratio of US than LS.

During a certain test stage, the consolidation degree of LS was the lowest among the four sampling locations. At the stage of SWC, the small hydraulic gradient in the soil at the bottom near the bucket wall led to a high pore ratio of LS. And under the vacuum pressure condition, the pore ratio of LS was large because it would take more time for the vacuum pressure to reach this part.

### 3.2.2. Pore Size Distribution

To describe the pores, the pore size needed to be defined. Here, the Expert Method (EM) was used to classify pores, and pore diameters of  $<0.04 \mu\text{m}$ ,  $0.04\text{--}0.4 \mu\text{m}$ ,  $0.4\text{--}4 \mu\text{m}$ ,  $4\text{--}40 \mu\text{m}$ , and  $>40 \mu\text{m}$  in the dredger fill were named the micropore, small pore, mesopore, large pore, and macropores, respectively [37]. Yuan et al. [30] used EM to describe the pore size change of the dredger fill during the SVP test, and proved its rationality in describing the pore size distribution of the dredger fill. The cumulative pore size distributions could be obtained based on the cumulative amount of mercury injection (Figure 8), and then the percentage of various types of pores could be determined (Figure 9).

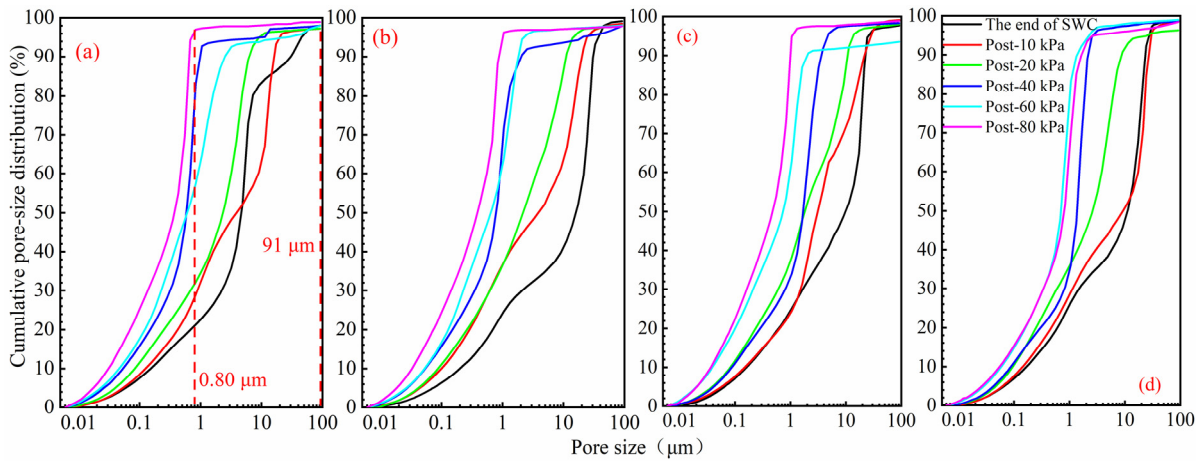


**Figure 8.** The curves of cumulative pore size distributions: (a) cumulative pore size distribution of samples from UC; (b) cumulative pore size distribution of samples from US; (c) cumulative pore size distribution of samples from LC; (d) cumulative pore size distribution of samples from LS.

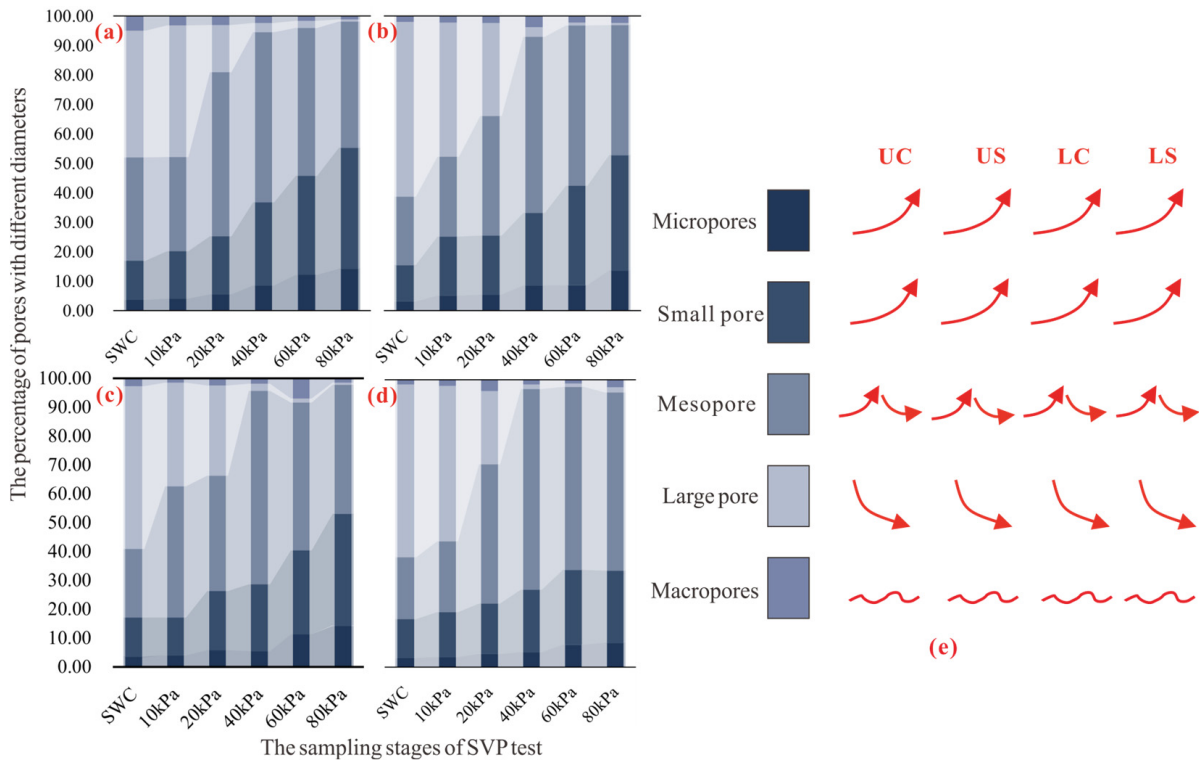


**Figure 9.** The percentage of pores with different diameters and its variation trend: (a) the percentage of pores with different diameters of UC; (b) the percentage of pores with different diameters of US; (c) the percentage of pores with different diameters of LC; (d) the percentage of pores with different diameters of LS; (e) the variation of different types of pores’ percentage during the SVP test.

The curves in Figure 8 indicate that the pore size became small with the increase in vacuum pressure. In Figure 8a, with the vacuum pressure increasing from 10 kPa to 80 kPa, the largest diameter of pore decreased from 91  $\mu\text{m}$  to 0.8  $\mu\text{m}$ . Figure 9 shows that the content of large pores decreased with the increase in vacuum pressure, while the contents of the small pores and micropores increased. The percentage of mesopores first increased and then decreased. The change in various types of pores implied that the large pores were mainly compressed into mesopores, small pores, and micropores during the consolidation of soil. When the vacuum pressure was 40 kPa, the mesopores’ content reached the peak

value. When the vacuum pressure was 60 kPa and 80 kPa, the content of small pores and micropores increased, but the mesopores content decreased. So, under a high vacuum pressure, the mesopores were compressed into small pores and micropores.

In the early testing stages, the percentage of large pores in the UC sample was the lowest, and it was the highest for the LS sample. At the end of the experiment, the percentages of large pores at the four sampling locations were almost the same, with a value of 0.75. The change in large pore content of samples from different positions showed a similar trend; it dropped rapidly under the first three levels of vacuum pressures, then decreased slowly under a vacuum pressure of 60 kPa and 80 kPa.

### 3.3. Correlation Analysis

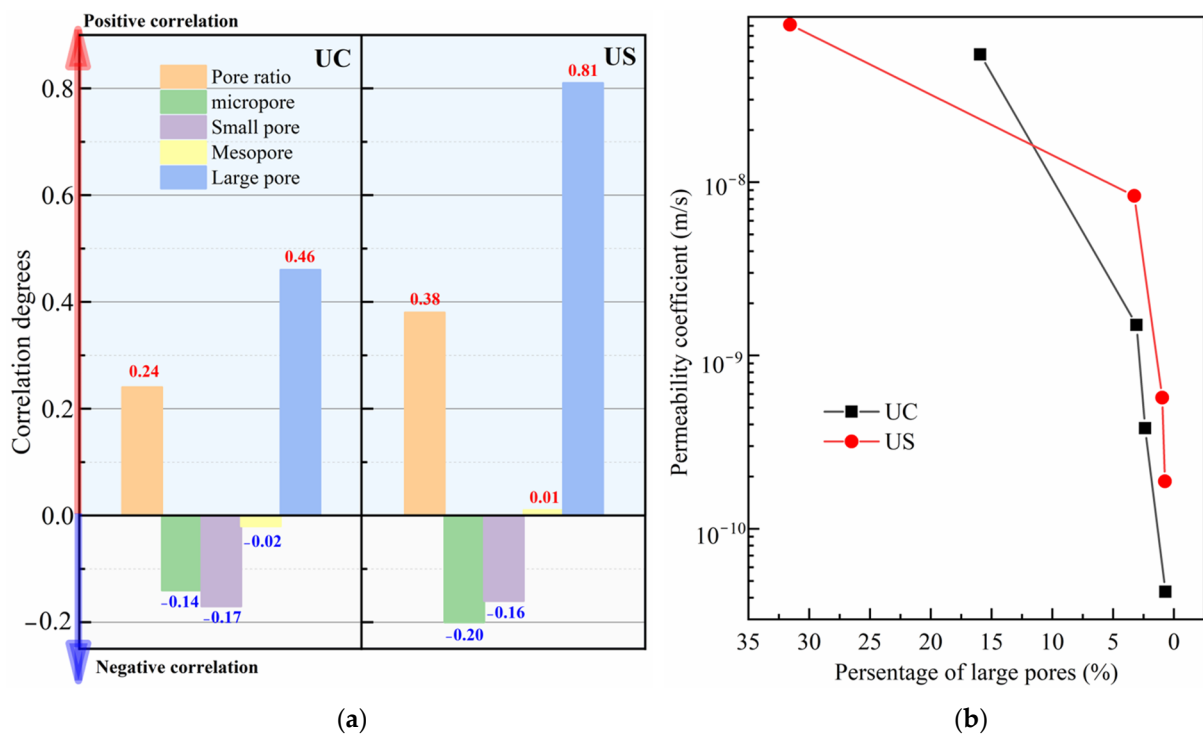
The pore ratio, percentage of large pore, mesopores, small pores, and micropores were selected as the comparison sequence, and the permeability coefficient of the soil was selected as the reference sequence. The selection of comparison sequence is consistent with permeability coefficient in terms of sampling location and testing stage. Table 3 lists the original data of the comparison sequence and reference sequence. Figure 10 lists the relationship between the pore parameters and the permeability coefficients.

Table 3. Original data: Reference sequence and comparison sequence.

| Testing Stage:<br>The Vacuum<br>Pressure Value | Sampling<br>Locations | Reference<br>Sequence             | Comparison Sequence |                  |                   |                 |                   |
|--|-----------------------|-----------------------------------|---------------------|------------------|-------------------|-----------------|-------------------|
|  |                       | Permeability<br>Coefficient (m/s) | Pore Ratio<br>(-)   | Micropore<br>(%) | Small Pore<br>(%) | Mesopore<br>(%) | Large Pore<br>(%) |
| 20 kPa   | UC                    | $5.46 \times 10^{-8}$             | 1.08                | 5.67             | 19.59             | 55.78           | 15.93             |
|  | US                    | $8.12 \times 10^{-8}$             | 1.19                | 5.39             | 20.14             | 40.49           | 31.58             |
| 40 kPa   | UC                    | $1.50 \times 10^{-9}$             | 0.76                | 8.60             | 28.20             | 57.78           | 3.07              |
|  | US                    | $8.34 \times 10^{-9}$             | 0.87                | 8.51             | 24.65             | 59.75           | 3.26              |
| 60 kPa   | UC                    | $3.80 \times 10^{-10}$            | 0.61                | 12.28            | 33.54             | 50.23           | 2.37              |
|  | US                    | $5.71 \times 10^{-10}$            | 0.76                | 8.64             | 33.79             | 54.39           | 0.96              |
| 80 kPa   | UC                    | $4.33 \times 10^{-11}$            | 0.54                | 14.27            | 41.10             | 42.81           | 0.7               |
|  | US                    | $1.88 \times 10^{-10}$            | 0.54                | 13.56            | 39.18             | 44.19           | 0.744             |

In Figure 10, the negative value of the correlation degree with an underline indicates that the permeability coefficient is negatively related to the comparison sequences. The larger the absolute value of the correlation degree, the stronger the correlation between the permeability coefficient and the comparison sequence. As shown in Figure 10a, the large pore content, pore ratio of soil samples in US and UC, and the mesopore content of soils in US exhibited a positive correlation with the permeability coefficient. The large pore content of the soil samples from US demonstrated the highest r value among these relationships. However, the content of small pores and micropores in the soil samples from US and UC, as well as the mesopore content of the soil samples from UC were negatively related to the permeability coefficient.

At different sampling locations, the r values between the permeability coefficient and the pore ratio were lower than that between the permeability coefficient and the large pore content. In the soil, the pore ratio represented the total volume of pore water that could exist, so the value of r between the pore ratio and permeability coefficient was slightly high. The large pore was the main seepage channel for water, and its percentage had the most direct influence on the permeability of the soil. Therefore, the value of r between the large pore content and the permeability coefficient was the highest.



**Figure 10.** The relationship between pore parameters and permeability coefficients: (a) the correlation degrees between pore parameters and permeability coefficients; (b) the relationship curves between the permeability coefficient and large pore percentage of the soil samples.

As shown in Figure 10b, the permeability coefficients decreased with the decrease in large pore contents. According to the analysis of pore size distributions, the large pore content was high after the SWC stage. Under the vacuum pressure, the large pores facilitated the drainage of pore water. So, the soil was compressed and consolidated. As shown in Figure 11, taking scanning electron microscope (SEM) photos of the soil samples at UC under different vacuum pressures as an example, the large pores were transformed into mesopores, small pores, and micropores during the application of vacuum pressure. With the decrease in large pore content, the size of the seepage channels for water became small, the permeability of the soil decreased under the increasing vacuum pressure, and the drainage capacity of the soil decreased. The large pore content decreased significantly under pressures of 10, 20, and 40 kPa, as did the permeability coefficient. So, the strongest correlation was between the permeability coefficient and the large pore content.

The  $r$  between the large pore content of US and the permeability coefficient was greater than that of UC. The large pores of UC were compressed into mesopores, small pores, and micropores in the earlier stage of the SVP test. The large pore content of UC decreased from 15.93% to 0.7%. Meanwhile, the large pore content of US reduced quickly from 31.58% to 0.74%. The variation in large pore content of US was more significant than that of UC. So the large pore content of US had the largest correlation level.

The mesopore content of UC was negatively correlated with the permeability coefficient, but that of US presented a positive correlation. The correlation level was the sum of the proximity of the slope ratio between the comparison sequence and the reference sequence in the adjacent time. The mesopore content presented different trends before and after 40 kPa, while the permeability coefficient declined throughout the test, indicating that the mesopore content had a negative or positive correlation with the permeability coefficient at different testing stages. When the sum of the absolute value of the negative results was larger than the sum of the positive ones,  $r$  was negative; otherwise,  $r$  was positive.

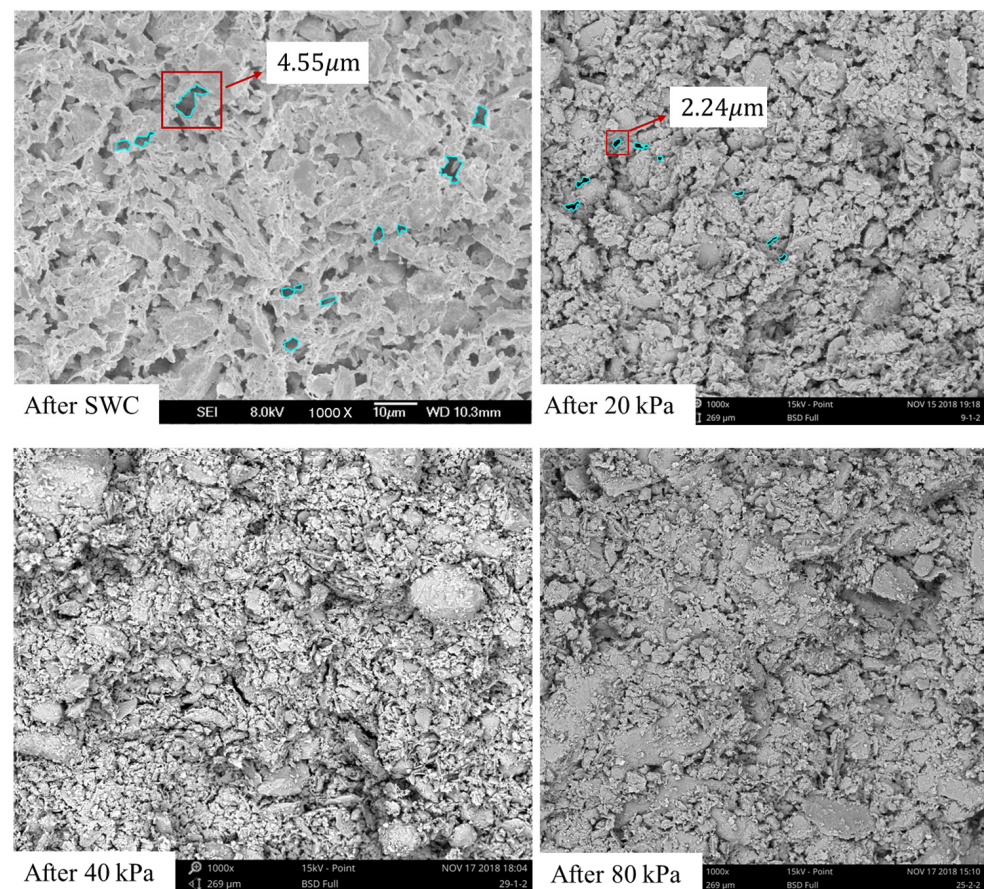


**Figure 11.** The SEM photos of soil samples from UC at the different sampling stages.

#### 4. Discussion

According to the above analysis, the percentage of large pores has a strong correlation with the characteristics of soil permeability. In this section, we use it to discuss the change in permeability coefficient of soil during the SVP test.

Figure 12 shows the variation in large pore content of soil samples with time and location. The large pore content of the samples at different locations decreases with the increasing vacuum pressure.

At the beginning of SWC, due to the differences in size and mineral composition of particles, the flocculation and sedimentation of particles in the stage of soil–water separation caused the following sorting: sand and silt concentrated at the bottom, and clay fraction filled in the space among large particles or was distributed in the upper part of the soil. The separated water connected with the permeable part of the PVD. When Valve 1 was opened, the separated water in the upper soil discharged rapidly through PVD under gravity, and the fine particles migrated to the vicinity of the PVD by the flow of water. Therefore, the large pore content of UC was the lowest because of the pore filling effect of the fine particles. So, the permeability of soil at UC was poor. In general, the large pore content was high at the end of the SWC stage at all four sampling locations, and the presence of large pores was beneficial for the discharge of pore water under the vacuum pressure.

Under a vacuum pressure of 10 kPa, the change in large pore content of UC was smaller compared with the change at the testing stage of 20 kPa and 40 kPa. This is because the vacuum pressure of 10 kPa was too small to cause an obvious change in large pores. Therefore, the permeability of the UC sample decreased slowly at the initial stage of vacuum preloading, which was conducive to the drainage of pore water far from the center. The large pore contents in the LC and US samples decreased more rapidly compared with that

in the LS samples. This discrepancy arose because it took time for vacuum pressure to transfer to the lower and marginal part of the soil, causing gradual consolidation of the deep soil far from the center. In contrast with the traditional vacuum preloading method, the SVP method utilizes a lower initial vacuum pressure when reinforcing dredger fill. These smaller pressures promote soil consolidation by restraining the migration of fine particles and preventing the blockage of PVD. This strategy is conducive to the discharge of pore water when higher vacuum pressures are subsequently applied, thereby improving the efficiency of soil consolidation.

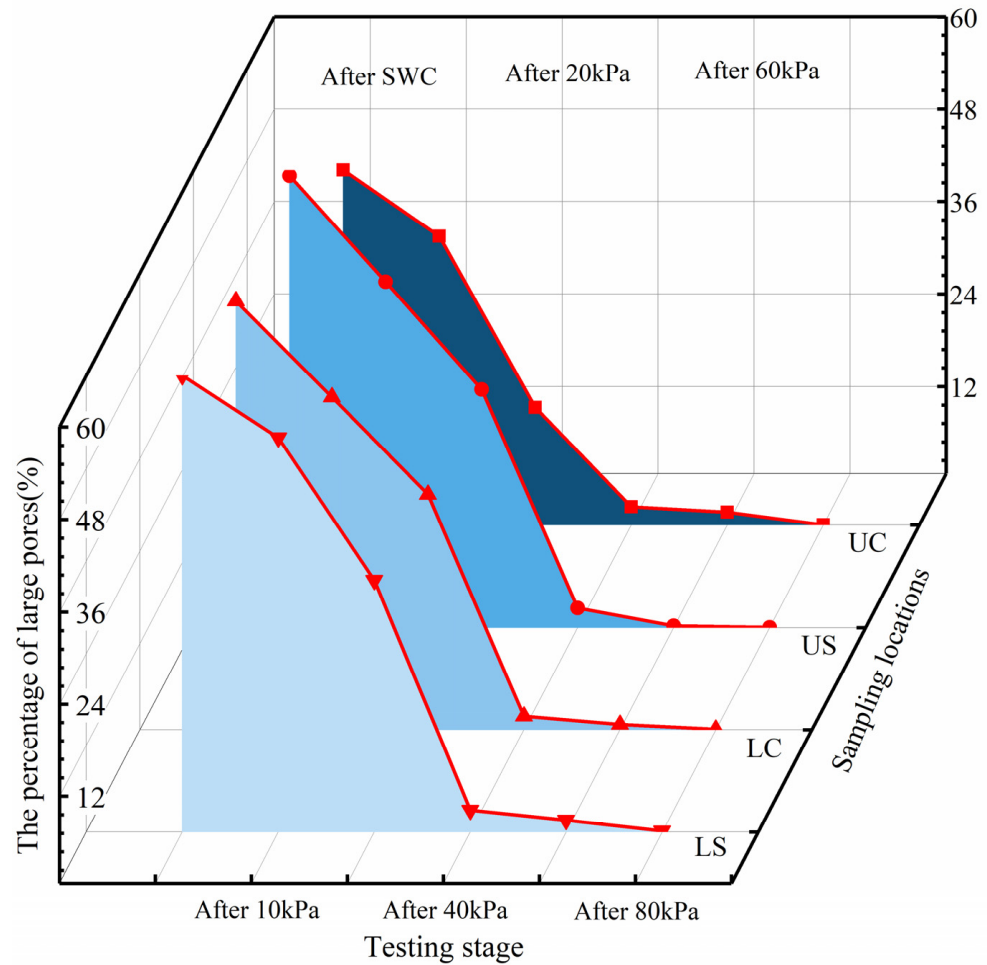


Figure 12. The large pore content of the soil samples.

When the vacuum pressure was 20 kPa, the change in large pore content of the four sampling locations increased. When the vacuum pressure was 40 kPa, the change decreased in the UC sample compared with that under the vacuum pressure of 20 kPa; but it increased in the US, LC, and LS samples. For the UC sample, at the end of SWC stage, it had the lowest large pore content compared with the samples from other three sampling locations, so after the reduction in large pore content under 10 kPa and 20 kPa vacuum pressures, it was difficult for the larger pore content of the UC sample to decrease continuously under 40 kPa vacuum pressure. During this stage, the mesopores content of the soil was the highest, and the large pore content was in the range of 2.40~3.60%. When the vacuum pressure was 60 kPa and 80 kPa, the change in large pore content was about 1%, but the contents of mesopores decreased quickly. The mesopores were transformed into small pores and micropores under high-level vacuum pressures of 60 kPa and 80 kPa. Due to the high vacuum pressure, the particle position constantly adjusted, resulting in the compact structure and low permeability coefficient of the soil.

The temporal and spatial variation of the pore characteristics and permeability coefficient showed the effectiveness of the SVP method in the reinforcement of high clay content dredger fill, and can provide a reference for the improvement of the reinforcement method.

## 5. Conclusions

The SVP test was conducted to consolidate dredger fill with a high clay content in the laboratory. Based on data obtained through MIP and permeability tests, the correlation between the pore parameters and permeability coefficient of soil was analyzed. The conclusions are as follows:

At the early stage of the SVP test, the permeability coefficient of soil samples decreased rapidly, followed by a slower decline as the pressure levels increased. The pore ratio of the samples from different locations decreased with the vacuum pressure. The pore ratio of the UC sample was the smallest, and it was the largest in the LS sample. Under a low vacuum pressure, the pore ratio decreased rapidly in the UC, US, and LC sampling locations. However, it became slow when the dredger fill was consolidated under vacuum pressure of 60 and 80 kPa. The pore ratio of the LS sample decreased with the vacuum pressure at a certain rate during the SVP test.

During the application of vacuum pressure, the large pores in the dredger fill gradually transformed into mesopores, small pores, and micropores. As the vacuum pressure increased to 60 kPa and 80 kPa, the mesopores were compressed into small pores and micropores.

The results of the correlation analysis indicate that among the various pore structure parameters, the large pore content demonstrated a strong correlation with the permeability coefficient of the soil. Therefore, the variation in large pore content with vacuum pressure could be used to describe the characteristics of soil permeability under vacuum pressure.

When acquiring soil samples for permeability tests becomes challenging, the permeability characteristics of the soil can be evaluated by analyzing the pore structure characteristics. The research results provide novel concepts for the establishment of permeability models, which could more accurately evaluate the settlement and stability of the soil during drainage consolidation.

**Author Contributions:** Conceptualization, H.-e.C.; methodology, H.-e.C. and W.S.; validation, H.-e.C., W.S., X.Y., X.L. and J.L.; formal analysis, W.S.; investigation, X.Y.; resources, X.Y.; data curation, X.L.; writing—original draft preparation, W.S.; writing—review and editing, W.S.; supervision, H.-e.C.; funding acquisition, H.-e.C., X.Y. and X.L. All authors have read and agreed to the published version of the manuscript.

**Funding:** This research was funded by the National Natural Science Foundation of China, grant number 42172301, 41602285, 51890914, and 42102346, respectively.

**Institutional Review Board Statement:** Not applicable.

**Informed Consent Statement:** Not applicable.

**Data Availability Statement:** The data will be shared upon reasonable request to the corresponding author.

**Conflicts of Interest:** The authors declare no conflict of interest.

## References

1. Kianfar, K.; Indraratna, B.; Rujikiatkamjorn, C. Radial consolidation model incorporating the effects of vacuum preloading and non-Darcian flow. *Géotechnique* **2013**, *63*, 1060–1073. [[CrossRef](#)]
2. Geng, X.; Yu, H.-S. A large-strain radial consolidation theory for soft clays improved by vertical drains. *Géotechnique* **2017**, *67*, 1020–1028. [[CrossRef](#)]
3. Lei, H.; Lu, H.; Liu, J.; Zheng, G. Experimental Study of the Clogging of Dredger Fills under Vacuum Preloading. *Int. J. Géoméch.* **2017**, *17*, 04017117. [[CrossRef](#)]
4. Yuan, X.-Q.; Wang, Q.; Lu, W.-X.; Zhang, W.; Chen, H.-E.; Zhang, Y. Indoor simulation test of step vacuum preloading for high-clay content dredger fill. *Mar. Georesour. Geotechnol.* **2017**, *36*, 83–90. [[CrossRef](#)]
5. Lei, H.Y.; Qi, Z.Y.; Zhang, Z.P.; Zheng, G. New Vacuum-Preloading Technique for Ultrasoft-Soil Foundations Using Model Tests. *Int. J. Géoméch.* **2017**, *17*, 04017049. [[CrossRef](#)]

6. Fang, Y.; Guo, L.; Huang, J. Mechanism test on inhomogeneity of dredged fill during vacuum preloading consolidation. *Mar. Georesour. Geotechnol.* **2019**, *37*, 1007–1017. [[CrossRef](#)]
7. Zheng, G.; Liu, J.; Lei, H.; Rahman, M.S.; Tan, Z. Improvement of very soft ground by a high-efficiency vacuum preloading method: A case study. *Mar. Georesour. Geotechnol.* **2017**, *35*, 631–642. [[CrossRef](#)]
8. Shan, W.; Chen, H.-E.; Yuan, X.; Ma, W.; Li, H. Mechanism of pore water seepage in soil reinforced by step vacuum preloading. *Bull. Eng. Geol. Environ.* **2021**, *80*, 2777–2787. [[CrossRef](#)]
9. Wu, Y.J.; Yang, J.B. Laboratory Model Tests on Dredger Fills by Vacuum Preloading with No Sand Cushion. *Appl. Mech. Mater.* **2012**, *170–173*, 655–660. [[CrossRef](#)]
10. Zhuang, Y.; Cui, X.Y. Evaluation of Vacuum Preloading with Vertical Drains as a Soft Soil Improvement Measure. *Soil Mech. Found. Eng.* **2016**, *53*, 210–217. [[CrossRef](#)]
11. Agus, S.S.; Leong, E.-C.; Rahardjo, H. Estimating permeability functions of Singapore residual soils. *Eng. Geol.* **2005**, *78*, 119–133. [[CrossRef](#)]
12. Saowapakpiboon, J.; Bergado, D.; Voottipruex, P.; Lam, L.; Nakakuma, K. PVD improvement combined with surcharge and vacuum preloading including simulations. *Geotext. Geomembranes* **2011**, *29*, 74–82. [[CrossRef](#)]
13. Bin Xu, B.; Liang, A.H.; Li, M.Y. Effect of Variable Permeability Coefficient on Consolidation of Ultra-Soft Ground under Vacuum Preloading. *Appl. Mech. Mater.* **2014**, *580–583*, 56–60. [[CrossRef](#)]
14. Sun, L.; Jia, T.; Zhuo, R.; Yan, S.; Guo, B. Numerical Solutions for Consolidation of Under-Consolidated Dredger Fill under Vacuum Preloading. *J. Coast. Res.* **2015**, *73*, 277–282. [[CrossRef](#)]
15. Indraratna, B.; Zhong, R.; Fox, P.J.; Rujikiatkamjorn, C. Large-Strain Vacuum-Assisted Consolidation with Non-Darcian Radial Flow Incorporating Varying Permeability and Compressibility. *J. Geotech. Geoenviron. Eng.* **2017**, *143*, 04016088. [[CrossRef](#)]
16. Baral, P.; Rujikiatkamjorn, C.; Indraratna, B.; Kelly, R. Radial consolidation characteristics of soft undisturbed clay based on large specimens. *J. Rock Mech. Geotech. Eng.* **2018**, *10*, 1037–1045. [[CrossRef](#)]
17. Nguyen, B.-P.; Kim, Y.-T. Radial consolidation of PVD-Installed normally consolidated soil with discharge capacity reduction using large-strain theory. *Geotext. Geomembranes* **2019**, *47*, 243–254. [[CrossRef](#)]
18. Sun, H.-L.; Weng, Z.-Q.; Liu, S.-J.; Geng, X.-Y.; Pan, X.-D.; Cai, Y.-Q.; Shi, L. Compression and consolidation behaviors of lime-treated dredging slurry under vacuum pressure. *Eng. Geol.* **2020**, *270*, 105573. [[CrossRef](#)]
19. Li, J.; Chen, H.; Yuan, X.; Shan, W. Analysis of the Effectiveness of the Step Vacuum Preloading Method: A Case Study on High Clay Content Dredger Fill in Tianjin, China. *J. Mar. Sci. Eng.* **2020**, *8*, 38. [[CrossRef](#)]
20. Kozeny, J. Ueber kapillare Leitung des Wassers im Boden. *Sitzungsber Akad. Wiss. Wien* **1927**, *136*, 271–306.
21. Carman, P.C. Permeability of saturated sands, soils and clays. *J. Agric. Sci.* **1939**, *29*, 262–273. [[CrossRef](#)]
22. Zhai, Q.; Rahardjo, H.; Satyanaga, A. A pore-size distribution function based method for estimation of hydraulic properties of sandy soils. *Eng. Geol.* **2018**, *246*, 288–292. [[CrossRef](#)]
23. Romero, E.; Gens, A.; Lloret, A. Water permeability, water retention and microstructure of unsaturated compacted Boom clay. *Eng. Geol.* **1999**, *54*, 117–127. [[CrossRef](#)]
24. Tuli, A.; Hopmans, J.W.; Rolston, D.E.; Moldrup, P. Comparison of Air and Water Permeability between Disturbed and Undisturbed Soils. *Soil Sci. Soc. Am. J.* **2005**, *69*, 1361–1371. [[CrossRef](#)]
25. Liu, Y.; Jeng, D.-S. Pore scale study of the influence of particle geometry on soil permeability. *Adv. Water Resour.* **2019**, *129*, 232–249. [[CrossRef](#)]
26. Zhai, Q.; Rahardjo, H.; Satyanaga, A.; Priono; Dai, G.-L. -L. Role of the pore-size distribution function on water flow in unsaturated soil. *J. Zhejiang Univ. Sci. A* **2019**, *20*, 10–20. [[CrossRef](#)]
27. Deng, Y.; Yue, X.; Liu, S.; Chen, Y.; Zhang, D. Hydraulic conductivity of cement-stabilized marine clay with metakaolin and its correlation with pore size distribution. *Eng. Geol.* **2015**, *193*, 146–152. [[CrossRef](#)]
28. Yuan, X.-Q.; Wang, M.-L.; Yan, H.; Chen, J.-Q.; Tan, B.-M. 3D Visualization Study on Microstructure Variation of Dredger Fill by Step Vacuum Preloading. In Proceedings of the GeoShanghai 2018 International Conference: Fundamentals of Soil Behaviours, Shanghai, China, 27–30 May 2018; Springer: Singapore, 2018; pp. 226–236. [[CrossRef](#)]
29. Liu, J.; Lei, H.; Zheng, G.; Feng, S.; Rahman, M.S. Improved Synchronous and Alternate Vacuum Preloading Method for Newly Dredged Fills: Laboratory Model Study. *Int. J. Géoméch.* **2018**, *18*, 04018086. [[CrossRef](#)]
30. Yuan, X.Q.; Wang, Q.; Sun, T.; Xia, Y.B.; Song, J. Pore distribution characteristics of dredger fill during hierarchical vacuum preloading. *J. Jilin Univ. Earth Sci. Ed.* **2012**, *42*, 169–176. [[CrossRef](#)]
31. Wang, J.; Cai, Y.; Fu, H.; Hu, X.; Cai, Y.; Lin, H.; Zheng, W. Experimental study on a dredged fill ground improved by a two-stage vacuum preloading method. *Soils Found.* **2018**, *58*, 766–775. [[CrossRef](#)]
32. Liu, Y.; Xiao, S.F.; Wang, Q. Research on indoor scale-down test of dredger fill. *Rock Soil Mech.* **2004**, *25*, 518–521. [[CrossRef](#)]
33. Luo, N.; Zhong, W.; Mei, S. Relational Analysis between Technological Progress and Economic Growth: An Empirical Study in Counties from Jiangsu Province. In *Advances in Grey Systems Research. Understanding Complex Systems*; Springer: Berlin/Heidelberg, Germany, 2010; pp. 165–176. [[CrossRef](#)]
34. Burdine, N. Relative Permeability Calculations from Pore Size Distribution Data. *J. Pet. Technol.* **1953**, *5*, 71–78. [[CrossRef](#)]
35. Garciabengochea, I.; Altschaeffl, A.G.; Lovell, C.W. Pore distribution and permeability of silty clays. *J. Geotech. Eng. Div.* **1979**, *105*, 839–856. [[CrossRef](#)]

36. Walker, R.; Indraratna, B. Consolidation analysis of a stratified soil with vertical and horizontal drainage using the spectral method. *Géotechnique* **2009**, *59*, 439–449. [[CrossRef](#)]
37. Wang, Q.; Wang, J.P. A Study on fractal of porosity in the soils. *Chin. J. Geotech. Eng.* **2000**, *22*, 496–498.

**Disclaimer/Publisher's Note:** The statements, opinions and data contained in all publications are solely those of the individual author(s) and contributor(s) and not of MDPI and/or the editor(s). MDPI and/or the editor(s) disclaim responsibility for any injury to people or property resulting from any ideas, methods, instructions or products referred to in the content.